

Perspectives on Gamma-Ray Pulsar Emission

Matthew G. Baring

*Department of Physics and Astronomy, MS-108, Rice University, P. O. Box 1892,
Houston, TX 77251-1892, USA Email: baring@rice.edu*

Abstract. Pulsars are powerful sources of radiation across the electromagnetic spectrum. This paper highlights some theoretical insights into non-thermal, magnetospheric pulsar gamma-ray radiation. These advances have been driven by NASA's *Fermi* mission, launched in mid-2008. The Large Area Telescope (LAT) instrument on *Fermi* has afforded the discrimination between polar cap and slot gap/outer gap acceleration zones in young and middle-aged pulsars. Altitude discernment using the highest energy pulsar photons will be addressed, as will spectroscopic interpretation of the primary radiation mechanism in the LAT band, connecting to both polar cap/slot gap and outer gap scenarios. Focuses will mostly be on curvature radiation and magnetic pair creation, including population trends that may afford probes of the magnetospheric accelerating potential.

Keywords: Pulsars; non-thermal mechanisms; magnetic fields; neutron stars; gamma-rays

PACS: 95.30.Cq; 95.30.Gv; 95.30.Sf; 95.85.Pw; 97.60.Gb; 97.60.Jd

INTRODUCTION

Prior to the launch of the Compton Gamma-Ray Observatory (CGRO) in 1991, the gamma-ray pulsar database was extremely limited. CGRO extended the population to seven sources, all of them young pulsars, and only Geminga had no definitive observation of a radio pulsar counterpart. There were also a few marginal CGRO detections, including the millisecond pulsar PSR J0218+4232. Following the launch of the *Fermi* Gamma-Ray Space Telescope on June 11, 2008, the gamma-ray pulsar database has grown rapidly, with over 75 sources now observed with high significance. Most of these are again young pulsars with higher spin-down luminosities than the average for radio pulsars. Yet, a sizable millisecond pulsar (MSP) population has emerged, at present numbering more than twenty. Moreover, the improved photon counts captured by the *Fermi* Large Area Telescope has enabled blind pulsation searches, those without prior knowledge of a radio timing ephemeris. The LAT has discovered over 20 pulsars in blind searches of the gamma-ray data alone, and only a few have since had radio confirmation.

The improved pulse-phase spectroscopy enabled by *Fermi* has clarified the probable locale of the gamma-ray emission region. The two major competing models for the site of this emission are the polar cap (PC) near the stellar surface (e.g. [10, 12]) and the outer gap (OG) near the light cylinder (e.g. [9, 20]). Super-exponential turnovers due to magnetic pair creation are expected for PC models at the maximum photon energies in the GeV band, as opposed to exponential shapes for OG models. Discrimination by *Fermi*-LAT between these two shapes was anticipated prior to launch [19]. In the vast majority of LAT pulsar spectra, the turnovers are exponential, thereby favoring the OG scenario [2]. Furthermore, the separation of peaks in pulsars with more than one pulse peak is generally of the order of 0.3–0.5 in phase, indicating a broad radiation

cone that is consistent only with high altitude emission locales for dipolar fields (e.g. [26]). This evidence has ushered in a new era for the γ -ray pulsar paradigm. Here, some perspectives pertaining to this new era are offered, focusing first on lower bounds to the emission radius from magnetic pair creation physics. In addition, the GeV-band turnover energies E_{MAX} are assessed in terms of the canonical radiation-reaction-limited curvature emission picture, touching upon population characteristics for γ -ray pulsars.

MAGNETIC PAIR CREATION BOUNDS FOR THE MINIMUM ALTITUDE OF EMISSION

The emergence of gamma-rays from pulsars is probably intimately coupled to the generation of electron-positron pairs in their magnetospheres. Such a connection between radiation emission and pair creation was posited in early radio-pulsar pictures [21, 24]. In the inner magnetosphere of young pulsars, the dominant pair production process involves a single photon interacting with the \mathbf{B} field, $\gamma \rightarrow e^+e^-$, with its non-magnetic, quantum counterpart $\gamma\gamma \rightarrow e^+e^-$ only becoming competitive at high altitudes. Hence, $\gamma \rightarrow e^+e^-$ is the preserve of *polar cap* (PC; [10]) and *slot gap* (SG; [18]) gamma-ray pulsar models. It is a first-order QED process that is kinematically forbidden in field-free regions, but can take place in an external magnetic field, which can absorb momentum perpendicular to \mathbf{B} . Its generic physics properties are summarized in [6]. Due to energy conservation, its rate R^{PP} possesses an absolute threshold energy, $\varepsilon_\gamma \geq 2/\sin\theta_{\text{KB}}$. Here θ_{KB} is the angle the photon momentum vector \mathbf{k} makes with the magnetic field \mathbf{B} , and the photon energy ε_γ is in units of $m_e c^2$, a convention adopted hereafter.

Above threshold, R^{PP} , which is averaged here over photon polarizations, exhibits a large number of resonances, corresponding to thresholds for the creation of pairs in excited states; these aggregate to exhibit a characteristic sawtooth structure (e.g. [6, 11]). In pulsar contexts, considerable ranges of field strengths and photon angles θ_{KB} are sampled during magnetospheric propagation: the resulting convolution smears out the sawtooth appearance into a continuum. In this regime, the dependence on ε_γ can be approximated by a compact asymptotic expression (e.g. [13]; and references in [6]):

$$R^{\text{PP}} \approx \frac{3}{8} \sqrt{\frac{3}{2}} \frac{\alpha_f c}{\lambda_c} \frac{B}{B_{\text{cr}}} \sin\theta_{\text{KB}} \exp\left\{-\frac{8}{3\Upsilon}\right\}, \quad \Upsilon \equiv \frac{B}{B_{\text{cr}}} \varepsilon_\gamma \sin\theta_{\text{KB}} \ll 1, \quad (1)$$

where Υ is the critical asymptotic expansion parameter. Here, $\alpha_f = e^2/(\hbar c)$ is the fine structure constant, $\lambda_c = \hbar/(m_e c) = 3.862 \times 10^{-11} \text{ cm}$ is the electron Compton wavelength over 2π , and $B_{\text{cr}} = m_e^2 c^3/(e\hbar) = 4.413 \times 10^{13} \text{ Gauss}$ is the quantum critical field, where the cyclotron energy equals $m_e c^2$. Near threshold, this asymptotic result is an imprecise description of R^{PP} [11], and can be improved considerably by careful treatment of the associated mildly-relativistic regimes for the produced pairs (e.g. [4]).

In polar cap pulsar models [10, 21, 24], primary curvature photon emission is emitted at very small angles to the magnetic field, well below pair threshold (e.g. [8]). These photons will convert into pairs only after traveling a distance s that is a fraction of the field line radius of curvature ρ_c . Above the polar cap, the radius of field curvature is $\rho_c = [Prc/2\pi]^{1/2}$ for a pulsar period P , and exceeds the neutron star radius R_{NS} . Pair

creation ensues for small angles such that $\sin \theta_{\text{KB}} \sim s/\rho_c$, and the argument Υ of the exponential becomes a fraction of unity, i.e., when $\epsilon_\gamma B \sin \theta_{\text{KB}} \gtrsim 0.2 B_{\text{cr}}$. Accordingly, in young pulsars, pair production will usually occur somewhat or well above threshold when $B \ll 0.1 B_{\text{cr}}$, and the attenuation mean free path $\lambda_{\text{pp}} \sim \rho_c/\epsilon \max\{2, 0.2 B_{\text{cr}}/B\}$ will then be much less than R_{NS} . Consequently, the optical depth $\tau_\gamma(\epsilon_\gamma)$ for one-photon pair opacity will be a *rapidly-varying function* of ϵ_γ , producing a dramatic attenuation signature at the escape energy ϵ_{esc} , which typically lies above 100 MeV (see [8]).

The upshot is that attenuation by $\gamma \rightarrow e^+e^-$ should impose a *super-exponential* cutoff in pulsar γ -ray spectra of the approximate form $dn_\gamma/d\epsilon_\gamma \propto \exp\{-\alpha \exp[-\epsilon_{\text{esc}}/\epsilon_\gamma]\}$ for some constant α . If $\epsilon_{\text{esc}} \sim \epsilon_{\text{MAX}} \equiv E_{\text{MAX}}/m_e c^2$, the severity of the cutoff should produce [10, 12] a sharp turnover that is distinguishable from those generated by other mechanisms. It was widely anticipated [19] that the *Fermi*-LAT instrument would discern the precise shape of such cutoffs in Vela and other pulsars, and accordingly discriminate between the polar cap and outer gap models for their high energy emission. It has in fact done so. Early on in the first year of observations by *Fermi*, the high count rates for Vela permitted the exclusion of super-exponential turnovers at a high level of significance [1]. This has become possible for the pool of 39 young pulsars listed in the *Fermi*-LAT Pulsar Catalog in [2], all of which reveal significant turnovers in the 1-10 GeV band consistent with simple exponentials. This clearly demonstrates that $\gamma \rightarrow e^+e^-$ is not producing the observed turnovers, proving that $\tau_\gamma(\epsilon_\gamma) < 1$ for $\epsilon_\gamma \lesssim \epsilon_{\text{MAX}}$.

This undeniable absence of the signature of active magnetic pair creation in gamma-ray pulsar signals can be inverted to provide robust lower bounds to emission altitudes, a protocol that has been adopted in a number of *Fermi*-LAT pulsar papers. Defining a marginal magnetic pair opacity criterion $\tau_\gamma(\epsilon_{\text{MAX}}) \approx 1$ near the pulsar surface, rearrangement yields an approximate dependence of pair creation cutoff energies ϵ_{MAX} on B_0 , R_0 and pulsar period P (in seconds). Setting $E_{\text{MAX}} \equiv \epsilon_{\text{MAX}} m_e c^2$, this can be summarized in a relation [5] that corresponds to near-surface emission ($r \lesssim 2R_{\text{NS}}$):

$$E_{\text{MAX}} \sim 0.4\sqrt{P} \left(\frac{r}{R_{\text{NS}}}\right)^{1/2} \max\left\{1, \frac{0.1 B_{\text{cr}}}{B_0} \left(\frac{r}{R_{\text{NS}}}\right)^3\right\} \text{ GeV} . \quad (2)$$

This encapsulates the character of accurate numerics derived from codes employed in [14] and [8], which include pronounced effects of general relativity on spacetime curvature, field enhancement and photon energy. In flat spacetime, the altitudinal dependence is weaker, corresponding to $\epsilon_{\text{MAX}} \propto (r/R_{\text{NS}})^{5/2}$ (e.g. [16, 27]) above the magnetic poles.

The pair opacity ϵ_{MAX} trend can be expressed alternatively as a combination of observables appropriate for this inner gap (polar cap) discussion. The form is

$$\log_{10} \frac{E_{\text{MAX}}}{1 \text{ GeV}} \approx \sigma_{\text{IG}} + \frac{7}{2} \log_{10} \chi_{\text{IG}} + 0.25 \quad , \quad \sigma_{\text{IG}} = -\log_{10} B_{12} + \frac{1}{2} \log_{10} P \quad . \quad (3)$$

which clearly encapsulates an anti-correlation with \dot{P} , as does Eq. (2), since $B_0 = 3.2 \times 10^{19} (P\dot{P})^{1/2}$ [17]. Here $\chi_{\text{IG}} = r/R_{\text{NS}}$ is the scaling of the radius appropriate for polar cap considerations. Figure 1 plots the phase space corresponding to Eq. (3), using the measured spectroscopic cutoffs E_c for young *Fermi*-LAT pulsars in Table 4 of [2] to

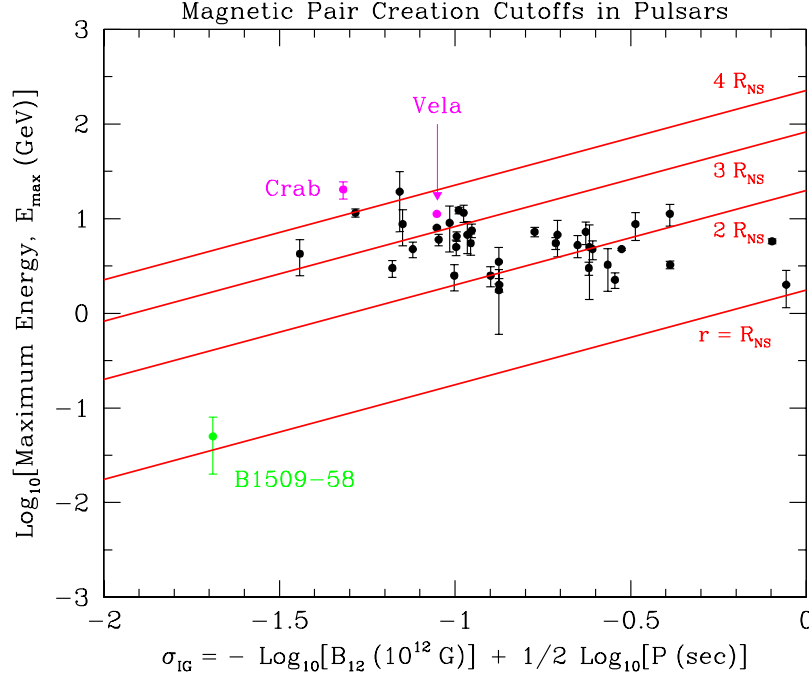


FIGURE 1. The inferred maximum pulsar emission energies E_{MAX} as a function of the key polar cap (inner gap) magnetic pair creation attenuation parameter σ_{IG} defined in Eq. (3). The spectral parameters used are the cutoff energies E_c listed in Table 4 of [2], the First *Fermi*-LAT Catalog of Gamma-ray Pulsars. For the 37 pulsars constituting the black points, $E_{\text{MAX}} = 2.5E_c$ was set; for the Crab and Vela, $E_{\text{MAX}} = 3.5E_c$ (see text). The high-field CGRO Comptel pulsar B1509-58 (J1513-5908) is also displayed. No LAT millisecond pulsars are depicted. The fiducial linear relationship in Eq. (3) is displayed as the diagonal lines for four different emission altitudes, $r/R_{\text{NS}} = 1$ (surface), 2, 3, 4, as labelled.

benchmark the maximum energies E_{MAX} . Since these cutoffs are exponential in character, the action of magnetic pair creation can be ruled out at energies below the window around E_c . For this reason, a representative setting of $E_{\text{MAX}} = 2.5E_c$ was deployed in the Figure for most of the pulsars, the set of 37 with points in black. This value can be adjusted on a case-by-case basis, depending on the photon counting statistics. Accordingly, the alternative value of $E_{\text{MAX}} = 3.5E_c$ was adopted for the Crab and Vela pulsars. Motivations for these exceptions are as follows: the Crab, possesses high energy emission reflected in its pulsed detection by MAGIC [3], and Vela, because its impressive count rate as the brightest LAT-band pulsar in the sky permits extraordinary spectroscopic determination of its turnover [1]. The uncertainties in E_c were scaled similarly, yielding the E_{MAX} error bars in the Figure. PSR B1509-58, the young, high-field pulsar detected by Comptel on CGRO, but not by EGRET, was also placed in the Figure using an inferred E_{MAX} value from the spectral results displayed in [14]. It is the only gamma-ray pulsar that might be consistent with $\gamma \rightarrow e^+e^-$ attenuation operating near the stellar surface. Observe that no millisecond pulsars (with $\sigma_{\text{IG}} < -2$) are exhibited in Fig. 1 as their surface fields are so low that $\gamma \rightarrow e^\pm$ pair creation is exponentially improbable in their magnetospheres. The phase space plot in Figure 3 clearly demonstrates that there is no correlation between ϵ_{MAX} and σ_{IG} or \dot{P} in the LAT pulsar population.

CURVATURE RADIATION AT HIGH ALTITUDES

Given the above discussion it is evident that the *Fermi* GeV-band spectral cutoffs in young pulsars are probably related to the primary emission mechanism. Dating from the early models of [24], this mechanism is postulated to be *curvature radiation*, the elementary dipole radiation resulting from pairs accelerating in the curved magnetospheric fields. The formalism for the curvature radiation emissivity is identical to that for classical synchrotron radiation [15, 22], but with the electron Larmor radius $r_L = \gamma_e m_e c^2 / (eB)$ being replaced by the radius of field curvature, ρ_c . Accordingly, the characteristic dimensionless (i.e., in units of $m_e c^2$) photon energy scales for curvature radiation, ε_c , and synchrotron emission ε_s , are

$$\varepsilon_c = \frac{3}{2} \gamma_e^3 \frac{\lambda_c}{\rho_c} \quad , \quad \varepsilon_s = \frac{3}{2} \gamma_e^3 \frac{\lambda_c}{r_L} \sin \theta_e \equiv \frac{3}{2} \frac{B}{B_{\text{cr}}} \gamma_e^2 \sin \theta_e \quad . \quad (4)$$

For curvature emission to seed pulsar gamma-ray signals, ε_c must exceed a few GeV in the magnetosphere; this is routinely satisfied in polar cap (e.g. [12]), slot gap [18] and outer gap (e.g. [20]) models, for both young pulsars and millisecond ones.

At its characteristic photon energy, the differential emissivity per electron scales as $\alpha_f c / \lambda_c \gamma_e^{-2}$ (e.g. see Eq. (2) of [7]) for both the curvature and synchrotron processes. When this emissivity scale is multiplied by the square of the photon energy scale in Eq. (4), the corresponding magnitudes for the curvature radiation and synchrotron cooling rates result; in full form these rates are

$$\dot{\gamma}_{\text{CR}} = -\frac{2}{3} \frac{r_0 c}{\rho_c^2} \gamma_e^4 \quad , \quad \dot{\gamma}_{\text{syn}} = -\frac{2}{3} \frac{r_0 c}{r_g^2} \gamma_e^2 \sin^2 \theta_e \quad . \quad (5)$$

Here $r_g = m_e c^2 / (eB) = \lambda_c B_{\text{cr}} / B$ is c divided by the cyclotron frequency, and $r_0 = \alpha_f \lambda_c = e^2 / (m_e c^3)$ is the classical electron radius. The precise numerical factors can be derived using the synchrotron formulation of [22]; for the curvature process this requires the specialization to pitch angles $\theta_e = \pi/2$. From Eq. (5) one derives the criterion for the *dominance of a synchrotron signal over a curvature one*: $\gamma_e \lesssim \rho_c \sin \theta_e / r_g$. While $\theta_e \approx 0$ is presumed for the primary emission, pair creation usually generates secondary photons at significant angles to the field, so that this inequality is almost always satisfied: synchrotron photons therefore abound in subsequent generations of a cascade. Since $\rho_c / r_g \gg 10^{15}$ near the polar cap in young pulsars, only very small θ_e are required to spawn the swamping of primary curvature emission by a synchrotron component in the inner magnetosphere. This possibility should be borne in mind for future refinements of the gamma-ray pulsar paradigm.

The maximum Lorentz factor of the electrons emitting in gamma-ray pulsars is a function of the accelerating potential adopted in a given model. If the electric field component along the local magnetic field is E_{\parallel} (presumed positive), then the energy gain rate in the electrostatic gap is $\dot{\gamma}_{\text{acc}} m_e c^2 = e E_{\parallel} c$, i.e. the electron speed c times the force. The maximum possible electron Lorentz factor γ_{MAX} is realized when this gain equals the loss rate due to radiative cooling, which is the *radiation-reaction limit* generally ascribed to curvature emission in gamma-ray pulsar models. Setting $-e E_{\parallel} / (m_e c)$ equal to

the first result in Eq. (5) yields a maximum e^- Lorentz factor $\gamma_{\text{MAX}} \sim [3\rho_c^2 E_{\parallel}/(2e)]^{1/4}$, which can then be inserted into Eq. (4) to specify the approximate maximum photon energy (in units of $m_e c^2$) for curvature radiation reaction-limited acceleration:

$$\varepsilon_{\text{MAX}} = \left(\frac{3}{2}\right)^{7/4} \lambda_c \rho_c^{1/2} \left(\frac{E_{\parallel}}{e}\right)^{3/4}. \quad (6)$$

This form for ε_{MAX} is routinely cited in *Fermi*-LAT publications on gamma-ray pulsars (e.g. [2]). In principal, the observed cutoff energy can be less than this value if attenuation by pair production, magnetic or two-photon, is efficient, or the acceleration is terminated by mechanisms other than curvature cooling. Hence, the observed GeV-band turnovers in dozens of young pulsars in the First *Fermi*-LAT Pulsar Catalog provide lower bounds to the accelerating potential, modulo the altitude of emission.

A natural, fiducial scale for the parallel electric field can be obtained from Lorentz transformations associated with a rotating magnetosphere. This establishes $r\vec{\Omega} \times \vec{B}/c$ as the co-rotational component of \vec{E} , providing the ideal MHD contribution. Yet within the plasmasphere, a non-co-rotational, parallel component E_{\parallel} emerges due to departures from Goldreich-Julian current flow (e.g. [23, 25]): it is putatively of the same order of scaling $\sim r\Omega B/c$. This is the most optimistic scenario, being adopted for example in the seminal outer gap pulsar model of [9], and leads to $E_{\parallel} \sim e/(r_0 \lambda_c) \chi^{-2} B_{\text{LC}}/B_{\text{cr}}$ for $\chi = r/R_{\text{LC}}$ describing the scaling of the acceleration/emission radius in terms of the light cylinder radius $R_{\text{LC}} = Pc/(2\pi)$ that will be employed hereafter. These define so-called thick outer gaps (e.g. [28]). Here B_{LC} is the field strength at $r = R_{\text{LC}}$, essentially along the last open field line. Note that the dependence of E_{\parallel} , B_{LC} and the radius of curvature on the obliquity of the rotator, and colatitude Θ , is omitted in this discussion. Using the scaled radius of curvature $v_c = \rho_c/(\chi R_{\text{LC}})$, one can then insert this nominal value for E_{\parallel} into Eq. (6). This can be cast in terms of observables P and \dot{P} . For a surface polar field $B_0 = 3.2 \times 10^{19} (P\dot{P})^{1/2} \equiv 10^{12} B_{12}$ Gauss and a neutron star radius of $R_{\text{NS}} = 10^6$ cm, since $B_{\text{LC}} = B_0 (R_{\text{NS}}/R_{\text{LC}})^3$, setting $P = 0.1 P_{-1}$ sec yields a result of

$$E_{\text{MAX}} \approx \frac{8.0 v_c^{1/2}}{\chi} (\varepsilon_{\parallel} B_{12})^{3/4} (P_{-1})^{-7/4} \text{ GeV} \quad (7)$$

This scaling is commensurate with that obtained in Eq. (4) of [20]. Clearly E_{MAX} rises monotonically as the acceleration locale moves from the light cylinder towards the neutron star surface, due to the rapidly rising inductive B -field. An additional *electrostatic decrement* factor $\varepsilon_{\parallel} \leq 1$ has been introduced in Eq. (7) to facilitate the subsequent discussion. It is an acceleration efficiency factor, representing the departure of E_{\parallel} below the fiducial, optimistic value of $E_{\parallel} \sim r\Omega B/c$; in general it is a function of the altitude parameter χ , the colatitude Θ and the rotator obliquity angle α .

To interpret this outer magnetospheric curvature radiation cutoff scaling, Figure 2 displays the phase space corresponding to Eq. (7), plotting $\log_{10} E_c$ versus the appropriate combination of observables P and \dot{P} ; in this graph, the cutoff energy E_c serves as a proxy for E_{MAX} . For the curvature radiation expectation in an outer gap (OG) near the

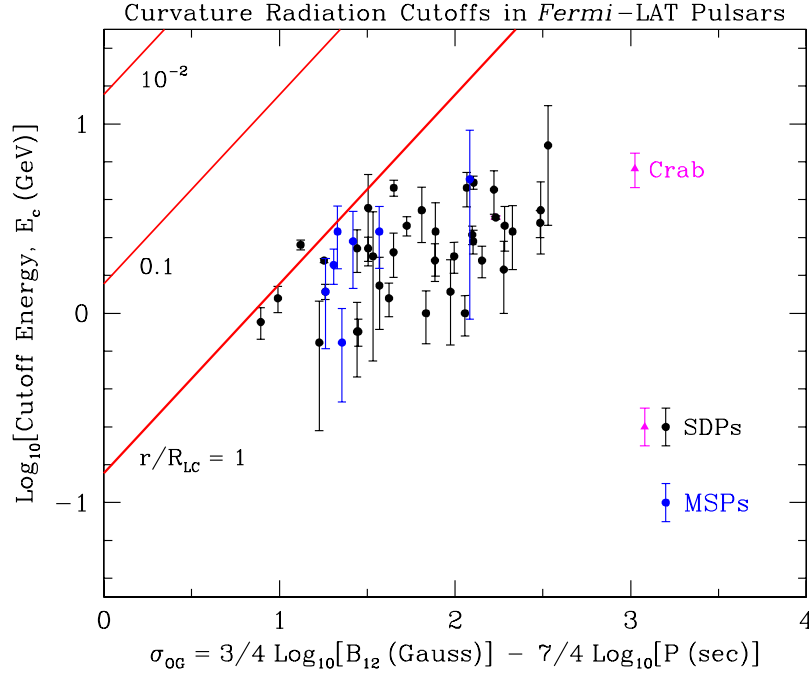


FIGURE 2. Observed *Fermi*-LAT pulsar emission cutoff energies as a function of the key outer gap curvature radiation reaction-limited acceleration parameter σ_{OG} defined in Eq. (8). The data come from the First *Fermi*-LAT Pulsar Catalog [2], with classic spinning-down pulsars (SDPs) in black, and millisecond pulsars (MSPs) in blue, as indicated. The Crab pulsar point from the *Fermi* dataset is highlighted, noting that its E_c from the MAGIC detection [3] is considerably higher. The diagonal lines labelled with $\chi = r/R_{\text{LC}}$ values constitute solutions of Eq. (8) for $\varepsilon_{\parallel} = 1$ and $v_c = 1$.

light cylinder, this is (for $\hat{\chi} = \chi v_c^{-1/2} \varepsilon_{\parallel}^{-3/4}$)

$$\log_{10} \frac{E_{\text{MAX}}}{1 \text{ GeV}} \approx \sigma_{\text{OG}} - \log_{10} \hat{\chi} - 0.85 \quad , \quad \sigma_{\text{OG}} = \frac{3}{4} \log_{10} B_{12} - \frac{7}{4} \log_{10} P \quad . \quad (8)$$

The graph is derived from the LAT pulsar data in Tables 1 and 4 of [2]. Since the E_{MAX} values appear in a relatively narrow range, with considerable spread in σ_{OG} , there appears to be no clear linear correlation, just the suggestion of one. The diagonal lines corresponding to $\hat{\chi} = 1, 0.1, 10^{-2}$ in the Figure provide an approximate guide to read off the scaled altitude. It is clear that this case of maximal E_{\parallel} cannot quite accommodate the turnover energies of the LAT pulsars being attributed to cooling-limited curvature emission within the light cylinder: the observations mandate that the electrostatic decrement lie in the range $0.05 \lesssim \varepsilon_{\parallel} \lesssim 1$ if $\chi = 1$. This essentially implies acceleration potentials somewhat weaker than the co-rotational benchmark $r\Omega B/c$, or considerably so (i.e., $\varepsilon_{\parallel} \lesssim 10^{-2}$) if the outer gap emission altitude lies well within the light cylinder radius, i.e. $\chi \lesssim 0.1$. This observational diagnostic becomes less constraining if some two-photon pair attenuation is active in the emission region, thereby lowering the observed cutoff energy E_c below the curvature radiation E_{MAX} .

The phase space plot in Fig. 2 exhibits a remarkable property — that the youngish, dipole-torque spin-down pulsars (SDPs) and old, recycled millisecond pulsars (MSPs) occupy the same locale. The x -coordinate, σ_{OG} , is an approximate linear function of $\log_{10} B_{\text{LC}}$, and the field B_{LC} is fairly similar for the two populations (see Table 1 of [2], and compare Fig. 2 here with their Figure 7 that displays the array of *Fermi*-LAT pulsar ε_{MAX} values versus $\log_{10} B_{\text{LC}}$). This approximate coincidence of B_{LC} values in SDPs and MSPs was, of course, well-known for the radio pulsar population. Yet, the clustering of the gamma-ray E_{MAX} around similar values for SDPs and MSPs is a new insight enabled by *Fermi*. It is strongly suggestive that similar physical acceleration locales and radiative emission mechanisms operate in the two populations.

Concluding Remarks: The picture of high altitudes for γ -ray emission in young pulsars is now well-established. Yet questions still remain. Is the primary mechanism curvature emission, or can small-angle synchrotron radiation contribute significantly to the signal? What is the role of two-photon pair creation in controlling the range of observed ε_{MAX} ? Does magnetic pair production at low altitudes still enhance the multiplicity of pairs being pumped into surrounding pulsar wind nebulae? These issues will capture the focus of theorists in the years to come as the *Fermi* pulsar legacy further unfolds.

REFERENCES

1. Abdo, A., et al. 2009, ApJ, 696, 1084.
2. Abdo, A., et al. 2010, ApJ Supp., 187, 460.
3. Aliu, E., et al. 2008, Science, 322, 1221.
4. Baring, M. G. 1988, M.N.R.A.S., 235, 51.
5. Baring, M. G. 2004, Adv. Space Res., 33, 552.
6. Baring, M. G. 2008, in Proc. CASYS '07 Conference *Computing Anticipatory Systems*, ed. D. M. Dubois (AIP Conf. Proc. 1051, New York), p. 53.
7. Baring, M. G. & Braby, M. L. 2004, ApJ, 613, 460.
8. Baring, M. G. & Harding A. K. 2001, ApJ, 547, 929.
9. Cheng K. S., Ho C. & Ruderman M. 1986, ApJ, 300, 500.
10. Daugherty, J. K. & A. K. Harding 1982, ApJ, 252, 337.
11. Daugherty, J. K. & Harding A. K. 1983, ApJ, 273, 761.
12. Daugherty, J. K. & Harding A. K. 1996, ApJ, 458, 278.
13. Erber, T. 1966, Rev. Mod. Phys., 38, 626.
14. Harding A. K., Baring, M. G. & Gonthier, P. L. 1997, ApJ, 476, 246.
15. Jackson, J. D. 1975, *Classical Electrodynamics* (Wiley and Sons, New York)
16. Lee, K. J., et al. 2010, M.N.R.A.S., 405, 2103.
17. Manchester, R. N. & Taylor, J. H. 1977, *Pulsars* (Freeman, San Francisco).
18. Muslimov, A. G. & A. K. Harding 2003, ApJ, 588, 430.
19. Razzano, M. & Harding, A. K. 2007, in *The First GLAST Symposium*, eds. S. Ritz, P. F. Michelson & C. Meegan (AIP Conf. Proc. 921) p. 413.
20. Romani, R. W. 1996, ApJ, 470, 469.
21. Ruderman, M. A. & Sutherland, P. G. 1975, ApJ, 196, 51.
22. Rybicki, G. & Lightman, A. 1979, *Radiative Processes in Astrophysics*, (Wiley & Sons, New York)
23. Shibata S. 1995, M.N.R.A.S., 276, 537.
24. Sturrock, P. A. 1971, ApJ, 164, 529.
25. Takata, J., Shibata, S., Hirotani, K. & Chang, H-K. 2006, M.N.R.A.S., 366, 1310.
26. Watters, K. P., Romani, R. W., Weltevrede, P. & Johnston, S. 2009, ApJ, 695, 1289.
27. Zhang, B. & Harding, A. K. 2000, ApJ, 532, 1150.
28. Zhang L. & Cheng K. S. 1997, ApJ, 487, 370.